Separation and fractionation of order and disorder in highly polydisperse systems

L. A. Fernández,[1,2] V. Martín-Mayor,[1,2] B. Seoane,[1,2] and P. Verrocchio[3,2]
[1]*Departamento de Física Teórica I, Universidad Complutense, Av. Complutense, 28040 Madrid, Spain*
[2]*Instituto de Biocomputación y Física de Sistemas Complejos (BIFI), Zaragoza, Spain*
[3]*Dipartimento di Fisica, Università di Trento, via Sommarive 14, 38050 Povo, Trento, Italy*
(Received 30 October 2009; revised manuscript received 7 May 2010; published 5 August 2010)

We study a polydisperse soft-spheres model for colloids by means of microcanonical Monte Carlo simulations. We consider a polydispersity as high as 24%. Although solidification occurs, neither a crystal nor an amorphous state are thermodynamically stable. A finite size scaling analysis reveals that in the thermodynamic limit: (a) the fluid-solid transition is rather a crystal-amorphous phase-separation, (b) such phase-separation is preceded by the dynamic glass transition, and (c) small and big particles arrange themselves in the two phases according to a complex pattern not predicted by any *fractionation* scenario.

DOI: 10.1103/PhysRevE.82.021501 PACS number(s): 64.70.D−, 64.75.Xc, 64.75.Gh

I. INTRODUCTION

Although in condensed matter physics spatial order is naturally linked to low temperatures, the presence of inherently disordered interactions (*quenched* disorder) challenges such scenario. The issue has been extensively addressed in lattice systems (spin glasses, magnetic materials in random field, etc.) where quenched disorder in fact inhibits spatially ordered structures (although not other types of order). Much less is known about off-lattice systems. The issue presents some practical consequences. For example crystallization of very viscous colloidal samples with size dispersion δ, see Eq. (1) below, larger than 12% does not occur, even after several months spent from the sample preparation [1]. This leads to several basic questions about the equilibrium phase diagram of polydisperse systems [2–10]. Does enough large polydispersity hinder crystallization? Is the glass phase stable rather than only metastable? Is there a dynamic interplay between crystallization and the glass transition [9,10]? And, probably at a more fundamental level, is thermodynamic equilibrium relevant at all to describe real polydisperse materials or these are instead inherently off-equilibrium over the experimental time scales? Answering such questions is crucial for condensed matter physics, since polydispersity is found both in artificial (synthetic colloids, polymers) and natural systems, from supercooled liquids on the atomic scale up to biological fluids such as blood.

An attempt to rationalize the experimental findings is the so-called terminal polydispersity scenario where a characteristic value $\delta_t \sim 0.12$ exists above which the homogeneous crystal becomes thermodynamically unstable. There is not consensus however about what kind of structure should replace such single phase crystal. Density functional analysis [7] predicts the instability of any crystal structure (even partial) above δ_t, thus leaving the amorphous ones (either liquid or solid) as the only possibility. Yet, the moment free-energy approach [5] predicts *fractionation*: phase separation between many crystal phases [though of the same ordering, face centered cubic (FCC), for instance], each one with a much narrower size dispersion than δ. Fractionation is supported by a recent numerical simulation that found that a first-order fluid-solid transition actually occurs at any polydispersity [8]. However, the solid phase is quite complex, at least in the high polydispersity region. In fact, for $\delta > 0.19$ the transition regards only a fraction of the particles and the ordered state is inhomogeneous. Such state has been previously referred to as I-phase [8].

Here we study the high polydispersity region, in particular the point $\delta = 0.24$. The corresponding $\delta - \beta$ phase diagram (β is the inverse temperature, $1/T$) is sketched in the inset in Fig. 3. This region is of great interest for various reasons. First, the amount of crystalline order for the coldest/densest configurations is unknown. It turns out to be phase-separated between a crystal and an amorphous state. The pattern of particle-size distribution among the two states does not follow any simple fractionation rule. Second, it has been suggested [8] that in this system the dynamic glass transition occurs in the stable rather than in the metastable fluid region. Our results support this claim in the large N limit. Besides, the detailed knowledge of the equilibrium structures is needed in order to design new experimental or numerical methods to drive the system toward such structures.

The layout of the rest of this work is as follows. In Sec. II we describe our model, the microcanonical ensemble (Sec. II A), and the considered observables (Sec. II B). Our simulation algorithm and our thermalization checks are described in Sec. III. Our main numerical results are described in Sec. IV. We present our conclusions in Sec. V.

II. MODEL

Take as a paradigm for polydisperse off-lattice systems the polydisperse soft spheres (PSS) model. We consider particles of radius σ_i, with $i = 1, 2, \ldots, N$. The particle size σ_i is drawn from a probability distribution function (pdf) $P(\sigma)$. Size polydispersity is in general characterized by a single parameter, δ, defined as the ratio among the standard deviation and the mean of $P(\sigma)$,

$$\delta = \frac{\sqrt{\langle \sigma^2 \rangle - \langle \sigma \rangle^2}}{\langle \sigma \rangle}. \tag{1}$$

At least for small polydispersity, δ seems to be the only feature of $P(\sigma)$ that controls the physical results.

 ©2010 The American Physical Society

Our particles interact via a pair potential,

$$V_{ij}(r) = \epsilon\left(\frac{1}{x_{ij}^{12}} + x_{ij} - \frac{13}{12^{12/13}}\right) \quad \text{if} \quad x_{ij} < x_c,$$

$$V_{ij}(r) = 0 \quad \text{if} \quad x_{ij} > x_c, \quad \text{with } x_{ij} = \frac{r}{\sigma_i + \sigma_j}, \; x_c = 12^{1/13}. \tag{2}$$

We take ϵ as energy unit. The potential is basically the repulsive part of Lennard-Jones, $1/r^{12}$. The only role of the linear piece is to provide a smooth long distance cutoff [11,12].

Our length unit, σ_0, is fixed by

$$\sigma_0^3 = \int \mathrm{d}\sigma_i \mathrm{d}\sigma_j P(\sigma_i) P(\sigma_j) (\sigma_i + \sigma_j)^3. \tag{3}$$

Although Eq. (2) generalizes well known models for simple liquids [13] (one would then choose $\sigma_0 \sim 1$ nm), the scale invariance of the $1/r^{12}$ potential suggests that our model may describe as well colloids. For the colloidal case one would choose $\sigma_0 \sim 1$ micrometer. In fact, the cutoff in the potential (2) makes it short ranged as it is appropriate for colloidal systems.

We simulated N particles in a box with periodic boundary conditions at density $\rho = \sigma_0^{-3}$. Due to the scale invariance of the $1/r^{12}$ potential, the thermodynamic parameter that controls the problem is the combination $\Gamma \equiv \rho T^{-1/4}$ (T is the temperature) [34].

Here we study the case where the size distribution is flat (constant in the range $[\sigma_{\min}, \sigma_{\max}]$). Sample-to-sample fluctuations are eliminated by picking the diameters in a deterministic way [8,14],

$$\sigma_i = \sigma_{\min} + (i-1)\frac{\sigma_{\max} - \sigma_{\min}}{N-1}. \tag{4}$$

Observe that

$$\delta = \frac{1}{\sqrt{3}}\frac{(r-1)}{(r+1)}, \quad \text{with } r = \frac{\sigma_{\max}}{\sigma_{\min}}. \tag{5}$$

Hence, $\sigma_{\max}/\sigma_{\min} \to \infty$ at $\delta_\infty = 1/\sqrt{3} \approx 0.57735$.

Since polydispersity hampers crystallization [1], a glass transition is to be expected. Although most of this work has been performed in the microcanonical ensemble, let us mention that we have also estimated the glass temperature in the (N,V,T) ensemble by means of Monte Carlo (MC) simulations. We simulated the equilibrium fluid state using only standard Metropolis single-particle moves (different choices of microscopic dynamics lead to basically equivalent results, see [15]). To locate the kinetic glass transition by computing the relaxation time τ of the fluid for $N = 500, 864$ in the range $\Gamma \in [1.3, 1.46]$ (data not shown). Our definition of the kinetic glass transition Γ_g corresponds to the point when τ surpasses the 10^6 MC steps. Both for $N = 500$ and 864 particles, we find that $\Gamma_g = 1.455(5)$.

The signification of Γ_g is rather different, depending on whether one is studying liquids (i.e., $\sigma_0 \sim 1$ nm) or colloids ($\sigma_0 \sim 1$ micrometer). In the colloidal case, a standard MC step corresponds roughly to 0.01 s of experimental time [16], so that $\tau \sim 10^6$ MC steps ~ 3 h of physical time and Γ_g corresponds to the experimental glass transition. On the other hand, for liquids 1 MC step is roughly equivalent to one picosecond. Thus, $\tau \sim 10^6$ MC steps $\sim 10^{-6}$ physical seconds, implying that Γ_g rather corresponds to the Mode Coupling transition [17]. Indeed, for most molecular and polymeric glass-forming liquids τ at the Mode Coupling temperature lies in the range $10^{-7.5}$ and $10^{-6.5}$ seconds [18].

A. Constant energy ensemble

We shall be working in the (N,V,E) ensemble. Specifically, we shall be using Lustig's microcanonical Monte Carlo [19] in the formulation of [20].

Let U be the total potential energy of our system,

$$U = \sum_{i<j} V(r_{i,j}), \quad (u \equiv U/N). \tag{6}$$

Thus, the total energy is

$$E = U + K, \quad (e \equiv E/N). \tag{7}$$

where $K = \Sigma_{i=1}^N p_i^2/2$ is the kinetic energy associated to the conjugated momenta $\{p_j\}$. Here, we are considering just one conjugated momentum per particle. As the kinetic energy is non-negative by definition, we should have $E \geq U$. The conjugated momenta are explicitly integrated out (they are simply a conceptual device to introduce the ensemble [19]).

A quantity of major importance in the microcanonical ensemble is the entropy density, $s_N(e)$,

$$\exp[N s_N(e)] = \frac{(2\pi N)^{N/2}}{N\Gamma(N/2)} \times \int \frac{\prod_{i=1}^N \mathrm{d}\boldsymbol{r}_i}{N!} (e-u)^{N/2-1} \theta(e-u). \tag{8}$$

The Heaviside step function, $\theta(e-u)$, enforces $e > u$. The microcanonical average of an arbitrary function of the particle positions $\{\boldsymbol{r}\}_i$ and of the energy density e, $O(\{\boldsymbol{r}\}_i; e)$ is defined as

$$\langle O \rangle_e \equiv \frac{\int \prod_{i=1}^N \mathrm{d}\boldsymbol{r}_i O(\{\boldsymbol{r}\}_i; e) \omega_N(\{\boldsymbol{r}\}_i; e)}{\int \prod_{i=1}^N \mathrm{d}\boldsymbol{r}_i \omega_N(\{\boldsymbol{r}\}_i; e)}, \tag{9}$$

where,

$$\omega_N(\{\boldsymbol{r}\}_i; e) = (e-u)^{N/2-1} \theta(e-u). \tag{10}$$

B. Observables

1. Inverse temperature

The main observable in a microcanonical simulation is the inverse temperature, computed as a microcanonical expectation value at fixed energy e,

$$\beta(e) \equiv \langle \hat{\beta} \rangle_e, \quad \hat{\beta} = \frac{N-2}{2N(e-u)}. \tag{11}$$

Note that

$$\beta(e) = \frac{\mathrm{d}s_N(e)}{\mathrm{d}e}. \tag{12}$$

The function $\beta(e)$ holds the key to connect the microcanonical formalism with the canonical one. Indeed, the *canonical* probability density for e, $P_\beta^{(N)}(e) \propto \exp[N(s_N(e) - \beta e)]$ can be recovered from $\beta(e)$,

$$\log P_\beta^{(N)}(e_2) - \log P_\beta^{(N)}(e_1) = N \int_{e_1}^{e_2} \mathrm{d}e(\beta(e) - \beta). \tag{13}$$

In the *thermodynamically stable region* (i.e., $\mathrm{d}\beta(e)/\mathrm{d}e < 0$), there is a single root of $\beta(e) = \beta$, located at the value of e where $P_\beta^{(N)}(e)$ is maximum. Instead, at phase coexistence there are several solutions for $\beta(e) = \beta$. Their interpretation is explained in Sec. IV A.

2. Particle-density field

As we mentioned in the Introduction, we expect large particle-density fluctuations. In order to detect them, we study the Fourier-transformed density field at the smallest, nonvanishing wave number allowed by the periodic boundary conditions:

$$\mathcal{F} \equiv \frac{1}{3}(|\hat{\rho}(2\pi/L,0,0)|^2 + \text{permutations}), \tag{14}$$

where L is the linear dimension of our cubic simulation box and the Fourier field is

$$\hat{\rho}(\boldsymbol{q}) = \frac{1}{N} \sum_i e^{i\boldsymbol{q}\cdot\boldsymbol{r}_i}. \tag{15}$$

Note that $\hat{\rho}(\boldsymbol{q})$, a function of the particles configuration, yields the static structure factor through $S(\boldsymbol{q}) = N\langle|\hat{\rho}(\boldsymbol{q})|^2\rangle$. In particular, $\hat{\rho}(0)$ is our nonfluctuating particle density ρ.

3. Crystalline order parameters

In order to study simultaneously crystallization and fractionation, we generalize the (rotationally-invariant) crystal order parameters [21,22] by measuring the crystal order only of a given set of particles $\mathcal{I}(x)$ (namely, particles whose index i verifies $|i - xN| < 0.05N$, hence only particles of similar size are considered):

$$Q_l(x) \equiv \left(\frac{4\pi}{2l+1} \sum_{m=-l}^{l} |Q_{lm}(x)|^2 \right)^{1/2}, \tag{16}$$

where (Y_{lm} are the spherical harmonics),

$$Q_{lm}(x) \equiv \frac{\sum_{\sigma_i \in \mathcal{I}(x)} q_{lm}(i)}{\sum_{\sigma_i \in \mathcal{I}(x)} N_b(i)}, \quad q_{lm}(i) \equiv \sum_{j=1}^{N_b(i)} Y_{lm}(\hat{r}_{ij}). \tag{17}$$

The index j in the latter sum runs over the $N_b(i)$ neighbors of the particle i and $\hat{r}_{ij}$ is the unit vector linking the position of particles i and j. Particles i and j are said to be neighbors if $\|\boldsymbol{r}_i - \boldsymbol{r}_j\| < \Delta$. In order to meaningfully fix the scale Δ, we considered the average number of neighbors as a function of Δ, finding a plateau. The height of the plateau is remarkably N-independent, but its *width* increases with N (so, the particular choice of Δ becomes less critical as N grows). We fixed the value $\Delta = 0.35$ (in units of the maximum cutoff for the potential $2\sigma_{\max}x_{\text{cut}}$), that lies in the plateau for all our values of N and for all our energies in the solid phase.

Since we let the fraction of particles be a finite fraction x of N the Q_l's are intensive quantities. In amorphous phases $Q_l(x)$ decrease as $1/\sqrt{N}$ while in crystalline ones they remain of order 1. In particular, we consider the case $l = 6$.

III. NUMERICAL ALGORITHMS AND THERMALIZATION TESTS

In order to study the fluid-solid phase transition we implement a microcanonical MC strategy [19,20]. Fixing the total energy density e, while the temperature and the potential energy fluctuate [see Eq. (11)], we follow the evolution from one phase to the other by studying e in the *energy gap* between the two phases. This strategy turned out to be essential to assess the first-order nature of the phase transition in disordered Potts models [23].

The peculiarity of the polydisperse models addressed here, as compared with Potts and similar models, is in that the phase transition actually corresponds to a phase separation. In fact, our low energy state is inhomogeneous [8]. Thus moving e from large values (fluid) to small ones (partly solid) we gently *accompany* the system during the growth of the spatially segregated regions. Although internal energy will not be the only reaction coordinate (see below), we have found useful to combine microcanonical MC with a modified parallel tempering (PT) algorithm [24,25].

For the sake of clarity, we divide the remaining part of this Section in three paragraphs: particle movements at fixed energy (Sec. III A), Parallel Tempering (Sec. III B), and thermalization checks (Sec. III C).

A. Particle movements at fixed energy

The particle moves at fixed energy were, with 50% probability, either standard Metropolis single-particle moves, or global swap attempts (modified for a polydisperse system). Let us recall that in a swap move, one attempts to exchange the position of two particles of different sizes [26]. Both for single-particle and for swap moves we compute the ratio of the microcanonical weights, defined in Eq. (10), for the new and the old configuration $\omega_N^{\text{old}}/\omega_N^{\text{new}}$. The new configuration is accepted with Metropolis probability $\min\{1, \omega_N^{\text{old}}/\omega_N^{\text{new}}\}$.

To fully describe the swap algorithm, we need to discuss how we choose the pair of particles, A and B, whose position we are trying to interchange. Note that one needs to balance two effects in polydisperse systems. The acceptance is larger the closer the two particle sizes are. However, exchanging very different particles produces a more significant effect when trying to equilibrate the system. Our compromise has been the following. We pick particle A with uniform prob-

TABLE I. Parameters of simulations and Maxwell construction. For each number of particles, N, we estimate two characteristic time scales τ_{FS} and τ_{SS} for the PT random walk in energy (see text), in units of PT attempts. We perform $10^5 N$ MC steps at fixed energy, then try a PT sweep. We also report the total length of our simulations in units of PT sweeps ($5\times 32\,000$ stands for 5 independent runs of 32 000 PT sweeps each). The energies chosen for the PT were evenly spaced $e_{i+1}-e_i=0.01$, in the intervals [0.95, 1.14] ($N=256$), [1.05,1.2] ($N=500$) and [1.08,1.19] ($N=864$). For $N=864$ we added to the PT energy list the values 1.115,1.125,1.135, and 1.145 in the fluid-solid energy gap. We also report the (inverse) critical temperature (and the associated $\Gamma_c=\rho\beta_c^{1/4}$), as well as the dimensionless surface tension $\Sigma\beta_c^N\sigma_0^2$, as computed from Maxwell's construction.

N	β_c	Γ_c	$\Sigma^{(N)}\beta_c^N\sigma_0^2$	τ_{FS}	τ_{SS}	L_{sim}
256	5.665(3)	1.5428(2)		317(15)	~20000	5×32000
500	5.432(5)	1.5267(3)	0.0035(2)	~1000	~15000	2×30000
864	5.162(4)	1.5073(3)	0.0088(4)	~7000		1×12000

ability over the N possibilities. We pick B with uniform probability among particles such that $|\sigma_B-\sigma_A|<0.2(\sigma_{\max}-\sigma_{\min})$. Particle B is accepted with probability 1 if $|\sigma_B-\sigma_A|>0.1(\sigma_{\max}-\sigma_{\min})$ or with probability 0.2 in the opposite case. In case of rejection, a new particle B is selected until a suitable candidate is picked. On the coexistence-line, swap moves reduce by three orders of magnitude the tunneling time between the fluid and the solid phase.

B. Microcanonical parallel tempering

In our parallel tempering simulations, several statistically independent copies of the system at different energies are simulated (fixed *energies* rather than fixed temperatures, as it is normally performed in standard PT [24,25]).

Each Monte Carlo time unit consists of two steps:

(1) For each copy of the system, we perform $10^5\times N$ particle move attempts at fixed energy (either single-particle displacements or particle-swap attempts). During this stage, each copy of the system is completely independent from the others.

(2) Copies of the system at neighboring energies try to exchange their particle configuration. We first try to sweep the two configurations at the lowest energy, afterwards the second lowest with third lowest, etc. In this way, the particle-configuration at the lowest energy has a chance of getting to the highest energy in a single sweep.

For the sake of clarity let us name A,B the two systems that are currently attempting to exchange their particle configuration. The exchange is accepted with probability

$$\min\left[1,\frac{\omega_N(\{\boldsymbol{r}_i^{(A)}\};e^{(B)})\omega_N(\{\boldsymbol{r}_i^{(B)}\};e^{(A)})}{\omega_N(\{\boldsymbol{r}_i^{(A)}\};e^{(A)})\omega_N(\{\boldsymbol{r}_i^{(B)}\};e^{(B)})}\right]. \tag{18}$$

The microcanonical weights ω_N are given in Eq. (10).

Further details on the simulation are summarized in Table I.

Let us finally note that the here used Monte Carlo method is quite similar to that of Refs. [12,27]. We briefly mention the main differences. First, particle swap at fixed energy was not used in Refs. [12,27]. Second, phase coexistence (and the related Maxwell construction) was not studied. Third, in the formulation of [27], one has a single copy of the system that performs a random walk in energy space: it is a sort of simulated annealing simulation [25], rather than our parallel tempering. Besides, the approximation $\beta(e)\approx(N-2)/[2N\langle(e-u)\rangle]$ is used, which coincides with Eq. (11) only up to corrections of order $1/N$. The formulation of [12] is somehow intermediate between simulated annealing and parallel tempering. The energy range of interest is spliced into non-overlapping subranges. Each copy of the system is assigned to an energy subrange, where it performs a simulated annealing. From time to time one uses parallel tempering to exchange the copies of the system attached to neighboring energy subranges.

C. Thermalization checks

A crucial issue of PT simulations is to ensure thermalization. Fortunately, a nice feature of PT is that it provides a sound thermalization check by controlling that all systems visit uniformly the whole range of energies [28].

At variance with the Potts case, phase coexistence *inside the energy gap* between a fluid and a solid is apparent from the pdf of the quantity $\mathcal{F}$, defined in Eq. (14). Our results are shown in Fig. 1, top. At values of e close to the transition, we identify two coexisting peaks. One of them is located at $\mathcal{F}\sim 1/N$, as expected for an homogenous fluid phase. On the other hand, the position of the large $\mathcal{F}$ maximum becomes N-independent (this is clearer at lower energies, see bottom panel in Fig. 1), as it should occur for an inhomogeneous solid. Such phase coexistence makes us to expect a large growth with N of the autocorrelation times [29]. Actually, the pdf for $\mathcal{F}$ at low energies (Fig. 1, bottom) displays a shoulder at large $\mathcal{F}$, which corresponds to even more inhomogeneous solids. Hence, the PT dynamics is ruled by two different processes: tunneling from fluid to solid, and a second tunneling to even more inhomogeneous configurations.

The random-walk in the energy space is best described through a PT time autocorrelation function (see Ref. [28] for details), that indeed can be fit to a double exponential for $N=256$ and $N=500$, see Fig. 2. Mind that the *time* in this correlation functions correspond to the time-unit defined in Sec. III B. It is not related to any physical time correlation.

As expected from the above discussion, we identify two different time scales in Table I, one associated to the coex-

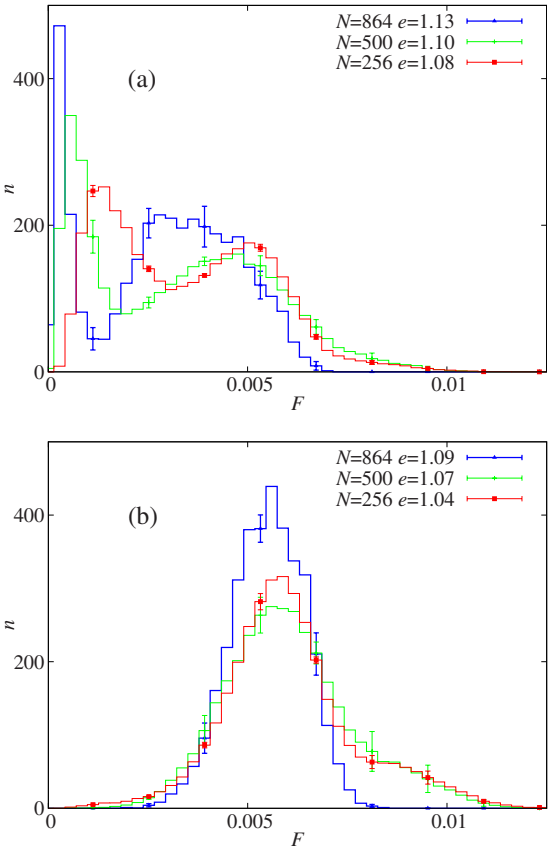

FIG. 1. (Color online) (pdf) of $\mathcal{F}$, Eq. (14) at various representative values of e. Data in panel (a) are computed at energy densities in the energy gap between the fluid and the solid phases. The double peak structure reveals phase coexistence (the position of the leftmost peak scales as $1/N$). Data in panel (b) are computed for e in the solid phase (the e-dependency there is very mild).

istence of the homogeneous and inhomogeneous phase, τ_{FS}, and a larger time, τ_{SS}, related to the more inhomogeneous configurations. For $N=864$, we could only identify the τ_{FS} scale. Probably, τ_{SS} is larger than the total time in our simulation. We remark that τ_{FS} for $N=256$ can be estimated with a 5% accuracy, while only the order of magnitude of τ_{SS} is

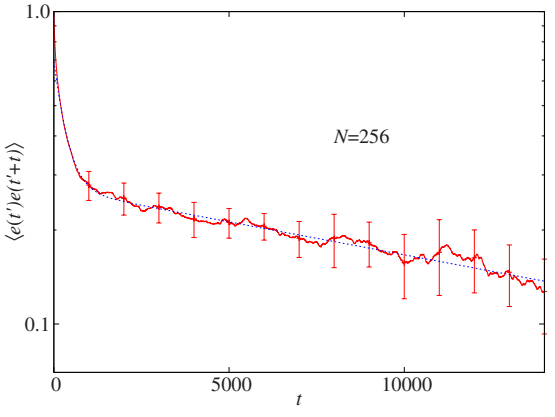

FIG. 2. (Color online) The (connected) time autocorrelation function for the energy in the PT can be fitted (dotted line) as $\langle e(t')e(t'+t)\rangle = a_{FS}e^{-t/\tau_{FS}} + a_{SS}e^{-t/\tau_{SS}}$.

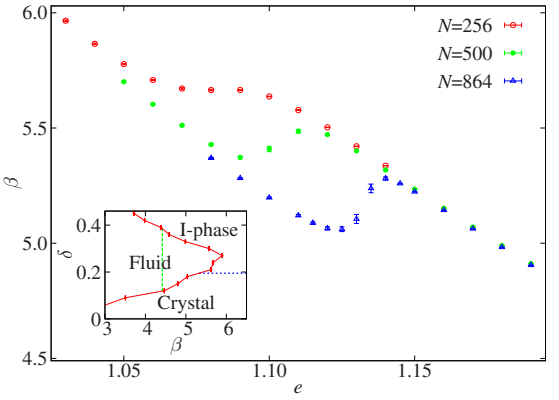

FIG. 3. (Color online) Finite size effects in the Maxwell construction. Main panel: the inverse temperature $\beta(e)$ as a function of the energy density e for various sizes of the sample. Inset: $\delta-\beta$ phase diagram of the system obtained from the data in Ref. [8].

determined. We have explicitly checked that the effects of these very inhomogeneous configurations on the Maxwell construction is fortunately smaller than our statistical errors [35]. Furthermore, from the point of view of our measured crystalline order parameters (see below), the more inhomogeneous configurations are not distinguishable from the main peak in the pdf.

IV. NUMERICAL RESULTS

A. Maxwell construction

As was mentioned in Sec. II B, in a microcanonical simulation, a quantity of major interest is the (inverse) temperature, $\beta(e)$, see Eq. (11). Thermodynamic stability requires that $\beta(e)$ be a decreasing function (i.e., positivity of the specific heat). Yet, see main panel in Fig. 3, this is not the case close to a first-order phase transition. The lack of monotonicity can be used to obtain the critical temperature, surface tension, etc. through Maxwell construction (see below, and Ref. [20] for details). Generally speaking, $\beta(e)$ has two distinct branches, one describing the fluid and the other the solid phase, where the specific heat $C_v \equiv -\beta^2 \mathrm{d}e/\mathrm{d}\beta$ is positive, connected by a thermodynamically instable line where $C_v < 0$. Although at finite N the system does not undergo a real phase transition, there are various criteria to define an (inverse) critical temperature, β_c^N, where the two different phases coexist with the same thermodynamic weight. Here we utilize the Maxwell construction, which amounts to obtain β_c^N as a solution of

$$0 = \int_{e_N^S(\beta_c^N)}^{e_N^L(\beta_c^N)} \mathrm{d}e(\beta(e) - \beta_c^N), \tag{19}$$

where the energy $e_N^L(\beta_c^N)$ $[e_N^S(\beta_c^N)]$ in turn corresponds to the rightmost (leftmost) root of the equation $\beta(e)=\beta_c^N$. Equation (13) shows that the Maxwell constructions amounts to the famous equal-height rule for the canonical probability-distribution function $P_\beta(e)$.

In Fig. 3 we show the function $\beta(e)$ for $N=256, 500, 864$. At odds with other models displaying a first

order transition, as N grows, both the supercooled fluid (fluid branch with $\beta > \beta_c^N$) and the overheated solid (solid branch with $\beta < \beta_c^N$) lines become longer.

As for the values of β_c^N reported in Table I, they decrease with N. Asymptotically, finite N corrections are of order $1/N$ (see [20] and references therein). A fit $\beta_c^N = \beta_c^\infty + a_1/N$ fails badly the χ^2 test. In other words, our estimates for β_c^N are accurate enough to resolve subleading scaling corrections in $1/N$. Thus, we have used a different approach. Let us assume that scaling corrections take the form of a smooth function in $1/N$, $\beta_c^N = \beta_c^\infty + a_1/N + a_2/N^2 + \cdots$. If we have at our disposal three values of N, we may compute a quadratic estimator (exact, up to corrections of order $1/N^3$),

$$\beta_c^{\infty,\mathrm{quad}} = \beta_c^{N_1} \frac{N_1^2}{(N_1 - N_2)(N_1 - N_3)} + \beta_c^{N_2} \frac{N_2^2}{(N_2 - N_1)(N_2 - N_3)} + \beta_c^{N_3} \frac{N_3^2}{(N_3 - N_1)(N_3 - N_2)}. \quad (20)$$

Computing the *statistical* error in $\beta_c^{\infty,\mathrm{quad}}$ is trivial, since $\beta_c^{N_1}$, $\beta_c^{N_2}$ and $\beta_c^{N_3}$ are statistically independent random variables. Using the data in Table I we get

$$\beta_c^{\infty,\mathrm{quad}} = 4.624(20), \quad \Gamma_c^{\infty,\mathrm{quad}} = 1.4664(15). \quad (21)$$

However, the quadratic polynomial in $1/N$ that interpolates our values $\beta_c^{N_1}$, $\beta_c^{N_2}$, and $\beta_c^{N_3}$ displays a maximum by $N \approx 256$, and decreases for smaller N. Hence, $\beta_c^{\infty,\mathrm{quad}}$ probably overemphasizes curvature effects. On the other hand, a linear (in $1/N$) extrapolation from $N_1 = 864$ and $N_2 = 500$ yields

$$\beta_c^{\infty,\mathrm{linear}} = 4.791(11), \quad \Gamma_c^{\infty,\mathrm{linear}} = 1.4795(9). \quad (22)$$

The correct thermodynamic limit probably lies in between of the two estimators $\Gamma_c^{\infty,\mathrm{quad}}$ and $\Gamma_c^{\infty,\mathrm{linear}}$, above the kinetic glass transition at $\Gamma_g = 1.455(5)$.

Furthermore, $\beta(e)$ also allows us to compute the surface tension [20],

$$\beta_c^N \sigma_0^2 \Sigma^{(N)} = \frac{N}{2L^{D-1}} \int_{e_N^*(\beta_c^N)}^{e_N^{\mathrm{L}}(\beta_c^N)} \mathrm{d}e (\beta(e) - \beta_c^N), \quad (23)$$

[recall that equation $\beta(e) = \beta_c^N$ has three solutions $e_N^{\mathrm{S}}(\beta_c^N) < e_N^*(\beta_c^N) < e_N^{\mathrm{L}}(\beta_c^N)$]. Data is shown in Table I.

B. Fractionation and crystalline ordering

The need for generalized order parameters, Eq. (16), follows from visual inspection of a typical $N = 864$ low-energy configuration, see Fig. 4. In fact, the smallest 400 particles (particle index $i < 400$) and some of the intermediates ($i \in [600, 725]$) show no sign of spatial order (bottom), while particles with $i > 725$ and $i \in [400, 600]$ form crystalline planes. Ordered and disordered particles fill different regions of the sample.

Our results in Fig. 5 confirm this picture. For $x < 0.45$ the crystalline order parameters decay as $1/\sqrt{N}$, while for $x = 0.55$ and $x = 0.95$ we obtain results roughly N independent. Thus, while the latter group of particles form a crystal (Q_6 is somewhat smaller than expected for FCC ordering), the former one remains amorphous. As for polydispersities, in the two-components crystal we estimate that $\delta \sim 0.15$, while in the fluid $\delta \sim 0.24$.

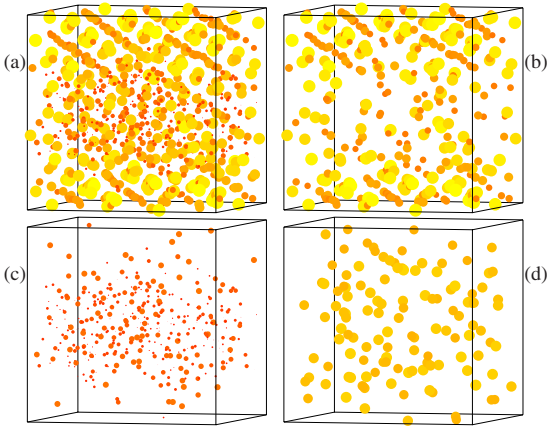

FIG. 4. (Color online) Snapshot of a typical low energy configuration ($N = 864$, $e = 1.01$). (a): whole system. (b): particles with index $i > 725$ and $i \in [400, 600]$. (c): particles $i < 400$. (d): particles $i \in [600, 725]$. The size of the circles are proportional to the particle sizes.

V. CONCLUSIONS

In summary, we have studied in the microcanonical ensemble a soft-spheres model for liquids and colloids with a 24% polydispersity. Extrapolating by finite size scaling (FSS) to the thermodynamic limit the results obtained from the Maxwell construction in finite systems, we show that the critical temperature for the amorphous-crystal phase-separation is *below* the dynamic glass transition, which makes dynamically difficult (although not impossible [10]) to observe such phase-separation.

At low temperatures the system divides spatially into an amorphous and a crystalline part, in agreement with previous findings [8]. The phase-separated amorphous is a stable fluid *below its dynamic glass temperature*, which is an optimal candidate to suffer a thermodynamic glass transition. On the other hand, the phase-separated solid displays crystalline order. Polydispersities on the coexisting amorphous and solid

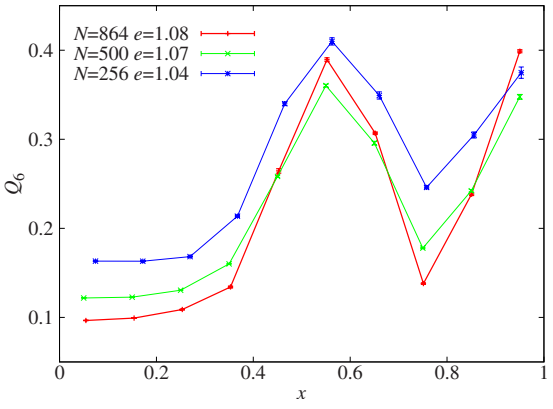

FIG. 5. (Color online) The crystal order parameter $Q_6(x)$, Eq. (16) as a function of the particles size x, for different N values.

are smaller than in the fluid. In fact, particles distribute spatially according to their size following a complex pattern not described by any fractionation scenario known to us. However, we must mention that there are strong similarities with the results of very recent isobaric semigrand canonical simulations [30]. Although restricted to smaller system sizes ($N=256$) and polydispersities ($\delta<7\%$ in the solid phase), these authors find as well that in the crystal phase the correlations between the fluctuating local particle-sizes extend to quite long spatial distances. Clearly enough, controlling finite-size effects is an important issue under such circumstances, and semigrand canonical simulation may prove useful in this respect.

ACKNOWLEDGMENTS

We acknowledge BIFI cluster and CINECA for 2×10^5 h of computer time. We have been partly supported through Research Contracts No. FIS2006-08533, No. FIS2009-12648-C03-01, and No. FIS2008-01323 (MICINN, Spain) and by UCM-Banco de Santander (Grant No. GR58/08). B.S. was supported by the FPU program (Spain).

[1] P. N. Pusey and W. van Megen, Nature (London) **320**, 340 (1986).
[2] P. Bartlett, J. Chem. Phys. **109**, 10970 (1998).
[3] D. A. Kofke and P. G. Bolhuis, Phys. Rev. E **59**, 618 (1999).
[4] S. Auer and D. Frenkel, Nature (London) **413**, 711 (2001).
[5] M. Fasolo and P. Sollich, Phys. Rev. E **70**, 041410 (2004).
[6] R. P. A. Dullens and W. K. Kegel, Phys. Rev. Lett. **92**, 195702 (2004).
[7] P. Chaudhuri, S. Karmakar, C. Dasgupta, H. R. Krishnamurthy, and A. K. Sood, Phys. Rev. Lett. **95**, 248301 (2005).
[8] L. A. Fernández, V. Martín-Mayor, and P. Verrocchio, Phys. Rev. Lett. **98**, 085702 (2007).
[9] G. Brambilla, D. El Masri, M. Pierno, L. Berthier, L. Cipelletti, G. Petekidis, and A. B. Schofield, Phys. Rev. Lett. **102**, 085703 (2009).
[10] E. Zaccarelli, C. Valeriani, E. Sanz, W. C. K. Poon, M. E. Cates, and P. N. Pusey, Phys. Rev. Lett. **103**, 135704 (2009).
[11] L. A. Fernández, V. Martín-Mayor, and P. Verrocchio, *The Xth International Workshop on Disordered Systems* (Taylor & Francis, New York, 2007), Vol. 87, pp. 581–586.
[12] Q. Yan and J. J. de Pablo, Phys. Rev. Lett. **90**, 035701 (2003).
[13] J. P. Hansen and I. R. McDonald, *Theory of Simple Liquids* (Academic Press, San Diego, 1986).
[14] L. Santen and W. Krauth, e-print arXiv:cond-mat/0107459.
[15] L. Berthier and W. Kob, J. Phys.: Condens. Matter **19**, 205130 (2007).
[16] N. B. Simeonova and W. K. Kegel, Phys. Rev. Lett. **93**, 035701 (2004).
[17] W. Gotze and L. Sjogren, Rep. Prog. Phys. **55**, 241 (1992).
[18] V. N. Novikov and A. P. Sokolov, Phys. Rev. E **67**, 031507 (2003).
[19] R. Lustig, J. Chem. Phys. **109**, 8816 (1998).
[20] V. Martin-Mayor, Phys. Rev. Lett. **98**, 137207 (2007).
[21] P. J. Steinhardt, D. R. Nelson, and M. Ronchetti, Phys. Rev. B **28**, 784 (1983).
[22] P. Rein ten Wolde, M. J. Ruiz-Montero, and D. Frenkel, J. Chem. Phys. **104**, 9932 (1996).
[23] L. A. Fernández, A. Gordillo-Guerrero, V. Martín-Mayor, and J. J. Ruiz-Lorenzo, Phys. Rev. Lett. **100**, 057201 (2008).
[24] K. Hukushima and K. Nemoto, J. Phys. Soc. Jpn. **65**, 1604 (1996).
[25] E. Marinari, in *Advances in Computer Simulation*, edited by J. Kerstész and I. Kondor (Springer-Verlag, Berlin, 1998).
[26] T. S. Grigera and G. Parisi, Phys. Rev. E **63**, 045102 (2001).
[27] Q. Yan, T. S. Jain, and J. J. de Pablo, Phys. Rev. Lett. **92**, 235701 (2004).
[28] L. A. Fernandez, V. Martin-Mayor, S. Perez-Gaviro, A. Tarancon, and A. P. Young, Phys. Rev. B **80**, 024422 (2009).
[29] D. P. Landau and K. Binder, *A Guide to Monte Carlo Simulations in Statistical Physics* (Cambridge University Press, Cambridge, England, 2000).
[30] P. Sollich and N. B. Wilding, Phys. Rev. Lett. **104**, 118302 (2010).
[31] B. Bernu, J. P. Hansen, Y. Hiwatari, and G. Pastore, Phys. Rev. A **36**, 4891 (1987).
[32] C. C. Yu and H. M. Carruzzo, Phys. Rev. E **69**, 051201 (2004).
[33] L. A. Fernández, V. Martín-Mayor, and P. Verrocchio, Phys. Rev. E **73**, 020501 (2006).
[34] Strictly speaking, the long distance cutoff spoils scale invariance, so that one could question that Γ is the controlling thermodynamic parameter. In practice, the cutoff is chosen to balance two mutually contradicting goals. On the one hand, the larger the cutoff distance, the lesser is the disturbance to the system. On the other hand, the computational cost significantly diminishes when one decreases the cutoff. Furthermore, the functional form of the cutoff is formulated to eliminate discontinuities, and thereby reduce its artificial effects. In fact, the Mode Coupling transition [17] has been located with a variety of cutoff choices and polydispersities (see [31–33] and present work). In all cases, when temperatures are expressed in terms of Γ, the location of the Mode Coupling transition Γ_g agreed to an accuracy of at least 1%.
[35] This is doing by following the random walk of each copy of the system in energy space. One easily realizes that, along the simulation, the system switches between *trapped* and ergodic phases. During a *trapped* phase, one or more copies of the system remains confined at the lowest energies and displays larger values of $\mathcal{F}$. In fact, the characteristic time τ_{SS} corresponds to the average duration of the trapped phase. The statistical analysis can be done either considering the full simulation or only the ergodic pieces of it. The Maxwell construction comes out compatible within statistical errors.